J. Chem. Thermodynamics 151 (2020) 106245

Contents lists available at ScienceDirect

J. Chem. Thermodynamics

journal homepage: www.elsevier.com/locate/jct

Measurement of the molecular dipole moment using active microwave thermography (AMT)

G.S. Grubbs II [a,*], A. Mirala [b], D. Bischof [b], M.T. Ghasr [c], K.M. Donnell [b]

[a] Missouri University of Science and Technology, Department of Chemistry, 400 W. 11th St., Rolla, MO 65409, USA
[b] Missouri University of Science and Technology, Department of Electrical and Computer Engineering, 301 W. 16th St., Rolla, MO 65409, USA
[c] Iowa State University, Department of Electrical and Computer Engineering, 2520 Osborn Dr., Ames, IA 50011-1046, USA

ARTICLE INFO

Article history:
Received 28 October 2019
Received in revised form 15 June 2020
Accepted 4 July 2020
Available online 8 July 2020

ABSTRACT

A method for implementing Active Microwave Thermography (AMT) for use in determining molecular dipole moments is reported. Specifically, the experimental setup along with a mathematical model for determining the dipole moment for deionized water is reported herein. The thermal and spatial resolution of the camera is shown to be of utmost importance in providing statistical and regional relevance, respectfully, of the properties of the material being studied. Deionized water in particular was studied in order to provide foundational knowledge for the veracity of using AMT in determining dipole moment values and representative values are reported herein. In order to extend the technique to more localized regions and composite systems, a more complex model and upgraded hardware are required.

1. Introduction

Active Microwave Thermography (AMT) refers to a measurement technique conventionally used for nondestructive testing and evaluation (NDT&E) purposes. It has recently shown promise for detection and evaluation of defects in numerous materials and structures including detection of cracks in corroded metals [1] and voids in carbon-fiber reinforced polymer (CFRP) structures [2], detection and evaluation of moisture ingress [3], health monitoring of structures coated with radar absorbing materials (RAM) [4], detection of delamination in layered structures [5,6], evaluation of steel fiber density in cement-based materials [7], and corrosion level on rebar [8], These applications show a high potential for AMT as an NDT&E tool.

AMT is based on the integration of microwave and thermographic NDT&E. More specifically, in AMT, microwave energy is utilized to heat a structure of interest, and the resulting surface thermal profile is monitored via a thermal/infrared (IR) camera. Compared to traditional (flash lamp) thermography, AMT does not require substantial amounts of power, and several (electromagnetic) parameters can be optimized in order to tailor the inspection to a specific material including frequency and polarization.

In general, when using a microwave-based thermal excitation, there are two possible heating mechanisms that may take place; dielectric heating and Joule heating. Dielectric heating takes place when the structure under test contains (lossy) dielectric materials. In general, the ability of a dielectric to generate heat is determined by its loss factor (ε'') which appears as the imaginary part of its complex dielectric constant ($\varepsilon = \varepsilon' - i\varepsilon''$). Due to the lossy electromagnetic properties of the material, microwave energy is absorbed and converted into heat. The real part of dielectric constant, on the other hand, represents the ability of the material to store electromagnetic energy. The other heating mechanism, Joule heating, occurs when conductive materials are present in the structure. When a conductor is exposed to electromagnetic radiation, depending on its electrical conductivity (σ), currents are induced inside the conductive material and ohmic losses occur. These induced currents can also serve as a secondary source of radiated energy which may cause subsequent dielectric heating in nearby dielectric materials. In all cases, the heat generated from the electromagnetic energy diffuses throughout the material via heat conduction. Besides the heat conduction, heat transfers to the environment by convection and radiation. These heat transfer mechanisms contribute to the heat distribution inside the structure.

Analyzing the surface temperature profiles captured during an AMT inspection allows the material under test to be characterized. Specifically, since dielectric materials can be polarized and absorb microwave energy, AMT may also be used as a materials characterization tool to determine properties such as the dipole moment. As such, this paper investigates, for the first time, the potential application of AMT to measure the dipole moment of materials. Since

* Corresponding author.
E-mail address: grubbsg@mst.edu (G.S. Grubbs II).

https://doi.org/10.1016/j.jct.2020.106245
0021-9614/

materials can be very complex, to show the utility of this approach, multiple volumes of a pure sample, deionized water (Table 1), was used, with the intention of expanding to other, more complex systems in the future. A rudimentary model has been implemented for the samples utilizing previous literature approaches [9–17]. Representative measurement results are provided for the deionized water samples, showing the potential of AMT for such applications.

2. Experimental setup

The AMT system schematic and experimental setup for the dipole moment measurements is illustrated in Fig. 1. The microwave radiation is generated using a low-power signal generator and amplified through a power amplifier. From this, a 50 W, 2.4 GHz signal is radiated toward the sample (mixture) using a horn antenna (aperture dimensions of 23×17 cm^2). This particular frequency was chosen due the sensitivity of water to signals at this frequency. In addition, this frequency is in the unlicensed frequency band allocated for industrial, scientific and medical (ISM) applications. The material under test was placed in a thermally insulating container (made of polystyrene) to avoid thermal losses from the bottom surface and sides. The container was also placed on a piece of microwave absorbing foam to avoid microwave energy reflecting back toward the sample and the antenna. The distance between the antenna and sample surface is referred to as the lift-off distance. The lift-off distance should be optimized to be small enough to ensure sufficient microwave radiation exposure on the sample and large enough to allow viewing of the sample surface with the thermal camera, and for this work was 15 cm. The microwave illumination and thermal measurement is controlled and synchronized with a data acquisition (DAQ) system and a computer using MATLAB™ software. The raw data are a collection of temperature measurement points made at the surface of the sample. In addition, thermal images are captured throughout the inspection time for real-time monitoring and stored for post-processing.

The horn antenna radiates microwave energy normal to the sample surface in order to maximize the microwave-induced heat over the surface. The thermal camera, however, has a skewed view of the sample surface. As such, the surface thermal profiles measured by the thermal camera are subsequently post-processed in order to remove the effect of the skew angle on the thermal images. Finally, the thermal camera used in this work is the FLIR T430sc, with the specifications shown in Table 2.

Measurements with water were conducted in two sets. In the first set, the heating time (when the mixture is under microwave illumination) and cooling time (when the microwave illumination is removed but the temperature is still being monitored) are 180 s each. For the second set of measurements, the heating and cooling times are 600 s each. In all the measurements in this work, the depth of the mixture is 5 mm. At this depth, 400 mL of sample volume are heated. Each measurement was repeated at least three times. The data from these measurements are then averaged (co-addition) in order to lower the noise level for smoother temperature variation curves. The AMT measurements are subject to noise from the environment (e.g., thermal energy from undesired sources reflected by the mixture and captured by thermal camera), emissivity variations over the inspection surface, thermal camera noise, etc.

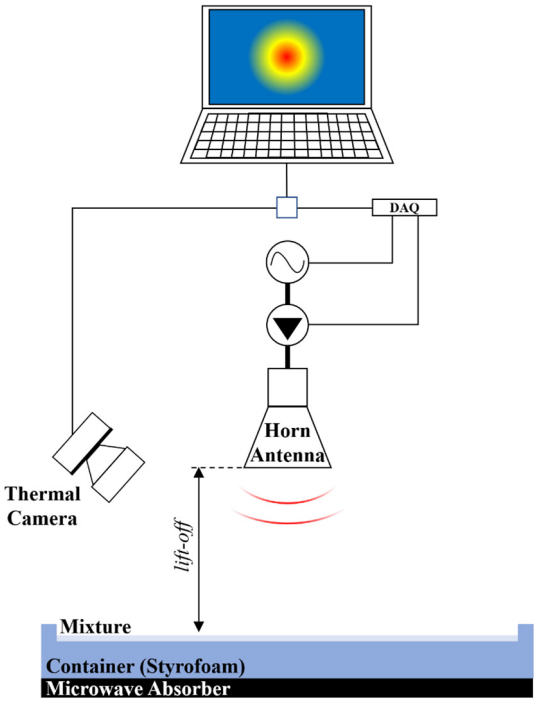

Fig. 1. The AMT system schematic and experimental setup for the dipole moment measurement of a mixture.

Table 2
Thermal camera specifications.

Parameter	Value
Detector type	Uncooled microbolomer
Wavelength band	7.5 – 13.0 μm
Detector size	320 × 240 px
Temperature resolution (NETD)	< 30 mK
Temperature range	−20°C – 120°C
Optics	Integrated lens 18 mm (25°)
Frame rate	30 Hz

3. Results

When illuminating a sample, the induced heat is directly related to the incident electric field (and consequently the incident power density) distribution at the sample surface (which is related to the horn antenna pattern and lift-off distance). One way to evaluate the incident power density distribution is to use a microwave absorber. In this case, the microwave absorber dissipates (absorbs) the incident power and its temperature rises proportionally to the incident power density. Fig. 2(a) shows the temperature increase of the microwave absorber, denoted by ΔT and defined as the difference between the temperature at a certain instance of time and the initial temperature prior to the onset of illumination, after 60 s of

Table 1
Sample Table.

Chemical		Initial Mole	Purification	Final Mole	Analysis
Name	Source	Fraction Purity	Method	Fraction Purity	Method
Deionized Water	DI Tap	–	Deionization	≤0.06 μS[a]	Conductance Measurement

[a] Probe used (microLAB® Model 160 Conductance Probe) has a cutoff at 0.06 μS and was reading 0.

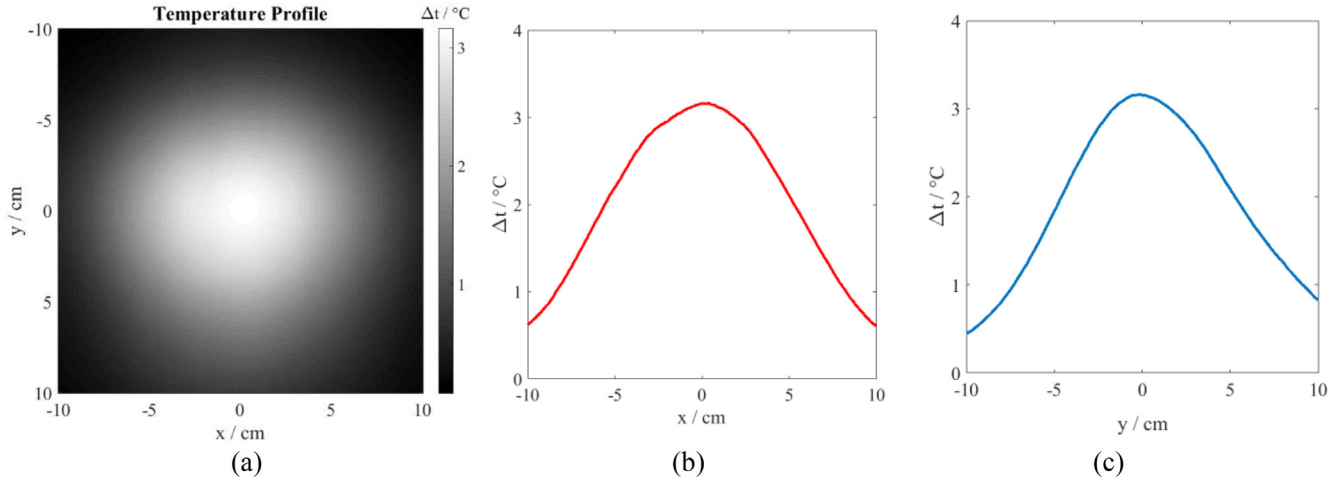

Fig. 2. The temperature distribution (a) over the surface and along the (b) x- and (c) y-axis of the microwave absorber after 60 s of microwave excitation.

microwave illumination and a lift-off of 15 cm. The microwave absorber is an 80 mil thick C-RAM FF-2/PPGA sheet. This absorber is a ferrite-filled silicone rubber sheet capable of absorbing 2.4 GHz microwave energy. As can be seen, the incident power is highly confined in an area with 5 cm radius over the absorber surface. Fig. 2(b) and (c) show ΔT as a function of position (x and y) across the middle of the absorber. As seen, the temperature has a Gaussian distribution along the two dimensions.

Fig. 3 shows the surface thermal profile at t = 180 s (left column), the temporal temperature change curve at the maximum of radiation exposure (beneath the center of the horn aperture) (middle column), and the spatial temperature variation curves on the x and y axes (right column). Additionally, these quantities are illustrated for the second set of measurements (with heating and cooling times of 600 s) in Fig. 4. During the heating period, the temperature increases since the absorbed microwave energy causes increase of temperature. The temperature increase rate, however, becomes slower over time because with increase of temperature, heat diffusion and convective and radiative heat transfer mechanisms start to sink the thermal energy from hotter places of the material. These mechanisms act to lower the temperature of hotter places down. Therefore, the temperature evolves slower (as the aforementioned mechanisms act opposite to the microwave heating). If heating is continued, the temperature will become constant everywhere and the thermal equilibrium takes place. Therefore, the temperature curve is expected to start rise rapidly initially after the microwave excitation is started and go into saturation over time. In the cooling period, on the other hand, only cooling mechanisms, i.e., thermal diffusion and convective and radiative cooling (act in the absence of microwave heating) and the temperature becomes more and more uniform over time. Finally, at very late times, the temperature becomes equal to the initial temperature when all the thermal energy induced by microwave heating and absorbed by the mixture is transferred into the environment. Moreover, the spatial distribution of temperature is expected to have almost a Gaussian shape since the heating pattern is Gaussian as discussed.

In order to better compare the measurement results of Figs. 3 and 4, ΔT (rather than absolute temperature) is shown in Fig. 5.

The post-processed thermal data is stored in an array of temperature measurements using MATLAB. This was done so that the camera's pixel resolution could be leveraged to give the most localized dipole moment values. As a result, the dipole moment values are only limited by the temperature and pixel resolution of the camera. Although the uncertainty of 30 mK in the thermal data is an upper limit as tabulated earlier, it was considered the best practice to consider this as the uncertainty in the thermal measurement. From this, a model was constructed utilizing the Onsager-Kirkwood-Fröhlich equation [12,16], as explained in the *Discussion* section below. This model was applied to deionized water and subsequently used to determine the localized dipole moment. MATLAB files programmed with the model that yield the dipole moment measurements are provided in the Supplemental Information.

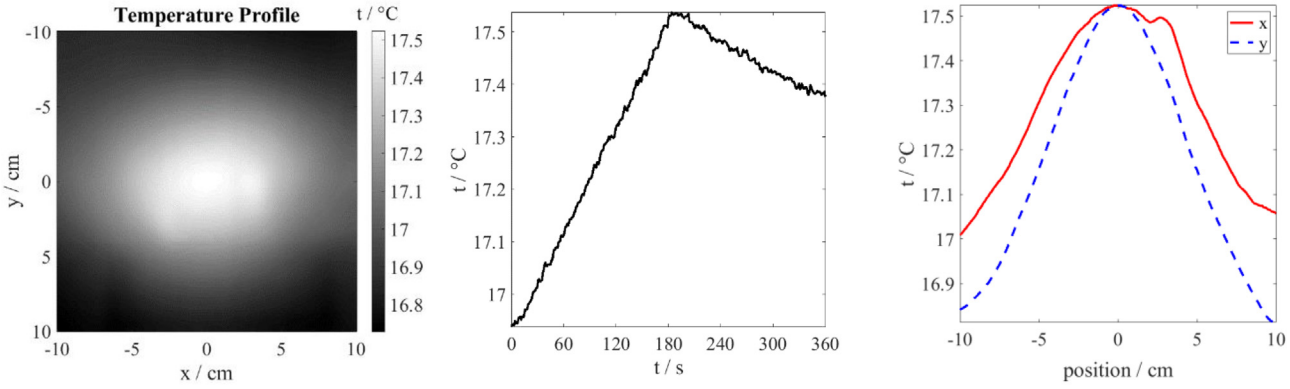

Fig. 3. The surface thermal profile (left) and temporal (middle) and spatial (right) distributions of temperature over the surface of deionized water after 180 s of microwave illumination.

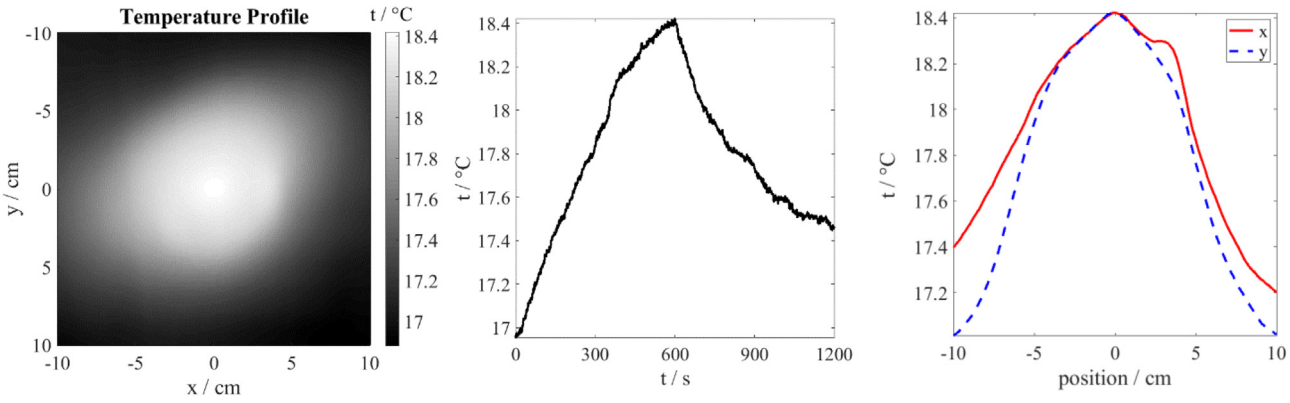

Fig. 4. The surface thermal profile (left) and temporal (middle) and spatial (right) distributions of temperature over the surface of deionized water after 600 s of microwave illumination.

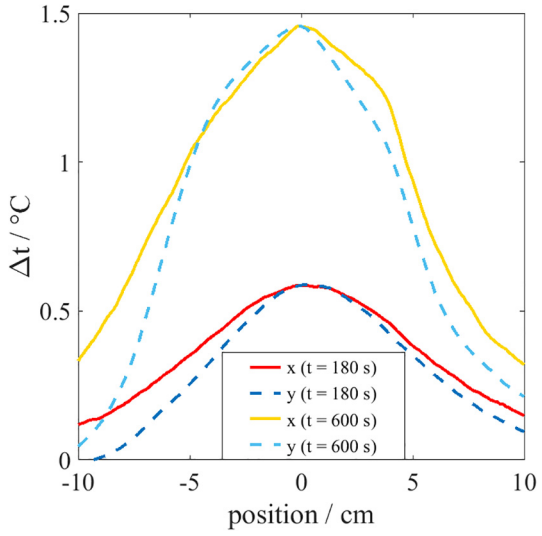

Fig. 5. Spatial variation of temperature rise after 180 and 600 s of microwave excitation over the surface of the deionized water.

4. Discussion

In order to interpret the resultant thermal data at a molecular level, the deionized water data set was analyzed as there is a significant amount of literature modeling the dipole moment from thermal data [9–21]. As this approach is intended to be the first step toward showing the veracity of using AMT for dipole moment monitoring, these initial tests did not necessarily monitor the field imposed on the samples but, rather, only the thermal response to this field. The particular models utilized by the authors focus on the Onsager-Kirkwood-Fröhlich equation, which results in a "free molecule" (or gas phase) dipole moment [12]:

$$\frac{(\varepsilon_s-\varepsilon_\infty)(2\varepsilon_s+\varepsilon_\infty)}{\varepsilon_s(\varepsilon_\infty+2)^2}=\frac{4\pi N_A\mu^2}{9V_mkT}g \tag{1}$$

In Eq. (1), ε_s is the static complex dielectric constant, ε_∞ is the high-frequency complex dielectric constant, N_A is Avogadro's number, V_m is the molar volume of the sample, k is the Boltzmann constant, T is the temperature of the sample, and μ is the permanent dipole moment of a "free molecule." The last variable, g, is the Kirkwood correlation factor defined by the mean of the orientation of the molecular dipole moments with respect to a singular dipole moment:

$$g=\langle\mu_i\cdot\sum_i\mu_i\rangle/\mu^2 \tag{2}$$

The g-value is generally given as a constant. This value is an issue of extreme importance in this model, but also one of extreme debate. As can be observed in the equation, the g-value is directly a function of the static dielectric constant, ε_s, and high-frequency dielectric constant, ε_∞. Because it is not frequency dependent, ε_s can be more easily measured and modeled [12]. However, ε_∞ is much more difficult to model as its value is frequency dependent. If only the electronic polarization is taken into account, however, this value takes on the index of refraction, n, squared, for a pure substance:

$$\varepsilon_\infty=n^2 \tag{3}$$

Since there is a difference in approach and difficulty to modeling pure and binary mixtures but still a need to show the veracity in using AMT for dipole moment measuring, the simplest scenario of employing a method to determine the molecular dipole moment (s) of a pure substance (deionized water) was evaluated. As such, this work is restricted to the pure substance of deionized water and extending the method and model to binary mixtures will be addressed in future works.

Fully understanding deionized water using the Onsager-Kirkwood-Fröhlich equation, however, is a well documented challenge in the literature. This problems/challenges arise from two factors: (i) the calculation of ε_∞, as mentioned above, and (ii) an assumed structure of the water molecule system originating from Onsager's original theory [22]. The empirical characterization of ε_s to a simple formula using a multitude of experimental methods greatly outweighed this concern. The empirical method of Uematsu and Franck utilize experimental data for water and steam ranging from 0 to 550 °C and pressures from 0.1 to 500 MPa [11]. This model uses the following equation for ε_s:

$$\begin{aligned}\varepsilon_s=1&+(A_1/T^*)\rho^*+(A_2/T^*+A_3+A_4T^*)\rho^{*2}\\&+\left(A_5/T^*+A_6T^*+A_7T^{*2}\right)\rho^{*3}\\&+\left(A_5/T^{*2}+A_9/T^*+A_{10}\right)\rho^{*4}\end{aligned} \tag{4}$$

where ρ^* is the adjusted density ratio, ρ/ρ_0, T^* is the adjusted temperature, T/T_0, ρ and T are the accepted density of 997.048 kg/m^3 for water from Ref. [23] and the measured temperature in K. T_0 and ρ_0 are 298.15 K and 1000 kg/m^3, respectively, while A_i is the corresponding equation coefficient which are all directly taken from Table 3 of Ref. [11]. The camera provides the raw temperature, T, and all other values are either standard values or determined from reference [11]. All experiments detailed here were performed in the

12–22 °C (285.15–295.15 K), and hence Table 3 shows the variance in ε_s of water in this temperature range according to the model. A spreadsheet of the derivation of these values is given in the Supplemental Information.

Table 3
Variance of the static complex dielectric constant, ε_s, with selected temperatures across the experimental region for water derived from Equation (4). Measurements of temperature are taken at the ambient room pressure of 0.980 bar (not controlled with regular fluctuations of ± 0.002 bar).

Temperature/ K	ε_s/ unitless
285.000 ± 0.030[a]	83.103
286.000 ± 0.030	82.739
287.000 ± 0.030	82.377
288.000 ± 0.030	82.017
289.000 ± 0.030	81.660
290.000 ± 0.030	81.304
291.000 ± 0.030	80.952
292.000 ± 0.030	80.601
293.000 ± 0.030	80.252
294.000 ± 0.030	79.906
295.000 ± 0.030	79.562

[a] Numbers in parentheses for temperature are reported as the maximum standard uncertainty (u, 0.68 confidence) in the measurement as reported by the thermal camera in Table 2.

Table 4
Calculation of the dipole moment, μ, across the heated water temperature gradients using derived ε_s values and representative temperature measurements in this study. The data are statistically significant to the fifth decimal place. Measurements of temperature are taken at the ambient room pressure of 0.980 bar (not controlled with regular fluctuations of ± 0.002 bar).

Temperature/ K	μ/ Debye
290.150 ± 0.030[a]	1.85239 ± 0.00003[b]
290.250 ± 0.030	1.85231 ± 0.00003
290.350 ± 0.030	1.85222 ± 0.00003
290.450 ± 0.030	1.85213 ± 0.00003
290.550 ± 0.030	1.85204 ± 0.00003
290.650 ± 0.030	1.85195 ± 0.00003
290.750 ± 0.030	1.85186 ± 0.00003
290.850 ± 0.030	1.85177 ± 0.00003
290.950 ± 0.030	1.85168 ± 0.00003
291.050 ± 0.030	1.85159 ± 0.00003
291.150 ± 0.030	1.85151 ± 0.00003
291.250 ± 0.030	1.85141 ± 0.00003
291.350 ± 0.030	1.85133 ± 0.00003
291.450 ± 0.030	1.85124 ± 0.00003
291.550 ± 0.030	1.85115 ± 0.00003

[a] Values for temperature are reported as the maximum standard uncertainty (u, 0.68 confidence) in the measurement as reported by the thermal camera in Table 2.
[b] Values for the dipole moment are reported from the maximum standard uncertainty (u, 0.68 confidence) in the temperature measurement.

The standardization of ε_s allowed us to calculate the dipole moment at each pixel using Eq. (1), taking the *g*-factor to be the general value of 2.82 and the high-frequency dielectric constant, ε_∞, as 1.78. The *g*-factor and ε_∞ are their usual values in this temperature range as detailed in reference [12]. Table 4 shows a sampling of the dipole moments calculated from 290.15 K to 291.55 K. These temperatures represent values observed with the camera while heating. The values are in good agreement with the accepted value of 1.85 D for water at room temperature [24]. Note that, due to the temperature resolution of the camera, the values are statistically different from each other in the fifth decimal place at the 1σ (68% confidence) interval, providing a very precise experimental measurement of the free molecular dipole moment.

2-D images of the dipole moment distributions at the water's surface were generated and shown in Fig. 6. The points generated give very precise measurements of dipole moments showing that, by following the heat distribution, the dipole moment measurement can be directly imaged with very good spatial (~1 mm^2) precision. Each point is calculated in the same manner presented above in the sample given in Table 4. Using the MATLAB program, we are able to isolate each point and generate a singular, statistically relevant dipole moment to create the image.

It should be noted that the model being used here, the Onsager-Kirkwood-Fröhlich equation, has been highly debated and criticized in the literature for inconsistencies in *g* and ε_∞, as well as the use of directly relating ε_∞ to n^2. Much of this problem, however, can be linked to localized molecular structure particularly dealing with complexation as the original works of Onsager assumed one possible structure of water and, from that, the resultant *g*-factor. As science has progressed, it has become apparent that water interactions can take on a multitude of structures in a variety of phases, which affect the calculated dipole moment value and, by extension, the *g*-value. In order to address this, deriving more accurate *g*-values for interacting species has become a developing trend in the literature as computational approaches become more sophisticated. However, using these more complex models is also unreliable because most assume a singular temperature. Coupling to these dipole moments with microwave energy for heating purposes will undoubtedly create localized complexation schemes that would also need to be monitored and/or calculated in order to get a more comprehensive and accurate understanding of the dipole moment.

It is hypothesized that this could also be accomplished with AMT if the system hardware and computational resources were improved. For example, with a higher resolution camera, more localized interactions could be monitored for their temperature

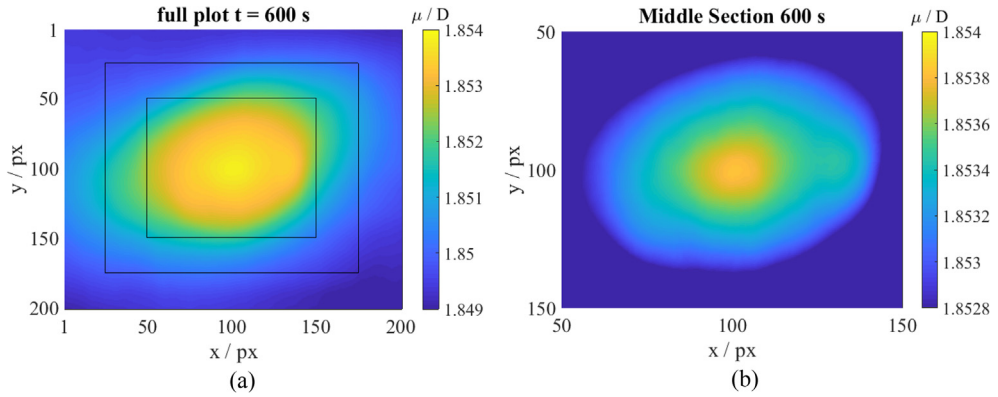

Fig. 6. Dipole moment spatial plots of the 600 s run. (a) The entire monitored area of the deionized water with denoted sections. (b) Innermost section of (a) showing that dipole value precision significance is preserved.

fluctuations. The imparted power and rate of heating could then be monitored in these local sections to provide a predicted response of the molecules based upon calculated and reported possible complexation structures of the molecular system of study. Doing the experiment in this way lessens the need for predetermined relationships in order to arrive at a dipole moment value, making the measurement more of an independent measurement that can be the basis of other experiments. The authors are currently pursuing these upgrades and adjustments in order to improve upon the instrument's very accurate dipole measurement capability.

5. Conclusions

These experiments show, when coupled with a model, AMT's ability to work as an *in situ* molecular dipole measurement technique for solutions. As this technique is inherently non-invasive, it also demonstrates the technique's ability to monitor systems undergoing change in real time without having to largely disturb the reaction vessel or system. These changes are can be monitored with very small temperature differences and very finite areas depending on thermal camera specifications. Since the heating is being accomplished through a coupling with the molecular dipole moment, these changes have measureable precision on these finite areas with statistical relevance to the free dipole moment value using simple modeling schemes. In order to get a more comprehensive and accurate understanding of localized dipole moments, however, some upgrades to the instrument and modeling scheme are required as microwave heating phenomena are very complex at all levels from bulk scale to molecular scale.

CRediT authorship contribution statement

G.S. Grubbs: Conceptualization, Methodology, Writing - original draft, Formal analysis. **A. Mirala:** Investigation, Software, Data curation, Methodology. **D. Bischof:** Software, Data curation, Visualization, Methodology. **M.T. Ghasr:** Supervision, Project administration, Funding acquisition, Resources, Methodology. **K.M. Donnell:** Supervision, Project administration, Funding acquisition, Writing - review & editing, Data curation, Resources, Methodology.

Declaration of Competing Interest

The authors declare that they have no known competing financial interests or personal relationships that could have appeared to influence the work reported in this paper.

Acknowledgements

This material is based upon work supported by the National Science Foundation under Grant No. ECCS-1609470.

Appendix A. Supplementary data

Supplementary data to this article can be found online at https://doi.org/10.1016/j.jct.2020.106245.

References

[1] A. Foudazi, A. Mirala, M.T. Ghasr, K.M. Donnell, Active microwave thermography for nondestructive evaluation of surface cracks in metal structures, IEEE Trans. Instrum. Meas. 68 (2) (2019) 576–585.
[2] A. Mirala, A. Foudazi, M.T. Ghasr, K.M. Donnell, Detection of flat-bottom holes in conductive composites using active microwave thermography, J. Nondestructive Eval. Diagn. Progn. Eng. Syst. 1 (4) (2018) 041005-1-7.
[3] A. Mirala, M.T. Ghasr, K.M. Donnell, In defect evaluation in active microwave thermography inspections, 27th American Society for Nondestructive Testing (ASNT) Research Symposium, Orlando, FL, 2018.
[4] A. Mirala, M.T. Ghasr, K.M. Donnell, In nondestructive assessment of microwave absorbing structures via active microwave thermography, Proceedings of the IEEE International Instrumentation and Measurement Technology Conference, Houston, TX, 2018.
[5] A. Mirala, X. Zou, M.T. Ghasr, L.H. Sneed, K.M. Donnell, In active microwave thermography: a real-time monitoring tool for CFRP-Concrete Bond Testing, Proceedings of the IEEE International Instrumentation and Measurement Technology Conference, Garden Grove, CA, 2019.
[6] A. Foudazi, M.T. Ghasr, K.M. Donnell, In Application of active microwave thermography to delamination detection, International Instrumentation and Measurement Technology Conference (I2MTC), 2014.
[7] A. Foudazi, I. Mehdipour, K.M. Donnell, K.H. Khayat, Evaluation of steel fiber distribution in cement-based mortars using active microwave thermography, Mater. Struct. 49 (12) (2016) 5051–5065.
[8] A. Foudazi, M.T. Ghasr, K.M. Donnell, Characterization of corroded reinforced steel bars by active microwave thermography, IEEE Trans. Instrum. Meas. 64 (9) (2015) 2583–2585.
[9] John G. Kirkwood, The dielectric polarization of polar liquids, J. Chem. Phys. 7 (1939) 911–919.
[10] Gerald Oster, John G. Kirkwood, The influence of hindered molecular rotation on the dielectric constants of water, alcohols, and other polar liquids, J. Chem. Phys. 11 (1943) 175–178.
[11] M. Uematsu, E.U. Franck, Static dielectric constant of water and steam, J. Phys. Chem. Ref. Data 9 (4) (1980) 1291–1306.
[12] O.A. Nabokov, Yu.A. Lyubimov, High-frequency dielectric constant of water and determination of the Kirkwood Correlation Factor, Zhurnal Strukturnoi Khimii 27 (5) (1986) 67–72.
[13] Donald G. Archer, Peiming Wang, The dielectric constant of water and Debye-Hückel limiting law slopes, J. Phys. Chem. Ref. Data 19 (2) (1990) 371–411.
[14] R.J. Sengwa, Vinita Khatri, Sonu Sankhla, Static dielectric constants and kirkwood correlation factor of the binary mixtures of N-methylformamide with formamide, N, N-dimethylformamide and N, N-dimethylacetamide, J. Solution Chem. 38 (2009) 763–769.
[15] M. Mohsen-Nia, H. Amiri, B. Jazi, Dielectric constants of water, methanol, ethanol, butanol and acetone: measurement and computational study, J Solution Chem 39 (2010) 701–708.
[16] R. João Carlos, Reis, T.P. Iglesisas, Kirkwood correlation factors in liquid mixtures from an extended Onsager-Kirkwood-Fröhlich equation, Phys. Chem. Chem. Phys. 13 (2011) 10670–10680.
[17] Mitja Drab, Ekaterina Gongadze, Luka Mesarec, Samo Kralj, Veronika Kralj-Iglič, Aleš Iglič, The internal and external dipole moment of a water molecule and orientational ordering of water dipoles in an electric double layer, Elektrotehniški Vestnik 84 (5) (2017) 221–234.
[18] A.P. Gregory, R.N. Clarke, Traceable measurements of the static permittivity of dielectric reference liquids over the temperature range 5–50 °C, Meas. Sci. Technol. 16 (2005) 1506–1516.
[19] Y. Daruich, C. Magallanes, L. Giordan, E. Garis, A. Catenaccio, Temperature dependence of the permittivity of some pure alcohols, Mol. Phys. 99 (2) (2001) 77–79.
[20] Anna V. Gubskaya, Peter G. Kusalik, The total molecular dipole moment for liquid water, J. Chem. Phys. 117 (11) (2002) 5290–5302.
[21] C. Magallanes, F. Vericat, A. Catenaccio, Kirkwood-Fröhlich correlation factor of methanol, Chem. Phys. Lett. 402 (2005) 428–432.
[22] Lars Onsager, Electric moments of molecules in liquids, J. Am. Chem. Soc. 58 (1936) 1486–1493.
[23] International Association for the Properties of Water and Steam, "Revised Release on the IAPWS Formulation 1995 for the Thermodynamic Properties of Ordinary Water Substance for General and Scientific Use (2018)" International Association for the Properties of Water and Steam: Prague, Czech Republic, 2018; Vol. IAPWS R6-95(2018) pp 1-19.
[24] Jr. Nelson, Ralph D., Jr. Lide, David R. and Arthur A. Maryott, Selected Values of Electric Dipole Moments for Molecules in the Gas Phase. United States Department of Commerce: 1967; p 49.